Fiber Front End with Multiple Phase Modulations and High-Bandwidth Pulse Shaping

Introduction

Since their first demonstration, lasers have led to incredible progress in many scientific and technological fields. High-intensity lasers have allowed researchers to explore new regimes for the interaction of light with matter. One far-reaching potential application of lasers is inertial confinement fusion (ICF), where nuclear fusion reactions are initiated by heating and compressing a deuterium–tritium (DT) target with laser beams. Large-scale laser facilities are in operation or in construction with the goal of demonstrating ignition,[1,2] following decades of research.[3] One difficulty of ICF is to maintain a high degree of spherical symmetry when the target is compressed: a spatially nonuniform on-target illumination can seed Rayleigh–Taylor instabilities at the target surface and detrimentally impact the fuel compression.[4] Smoothing by spectral dispersion (SSD) is an approach to reduce the spatial nonuniformities of the illumination generated by high-energy laser beams.[5] SSD lowers the coherence of the beams by frequency modulating them (i.e., increasing the optical-frequency content), spatially dispersing them with a diffraction grating (i.e., introducing a relation between optical frequency and wave vector), and focusing them after a random phase plate (i.e., creating a broad range of wave vectors in the near field and a speckle distribution in the far field).[6,7] The time-integrated far-field fluence of individual beams is smoothed because the phase plate generates randomly distributed speckles with a frequency-dependent distribution; consequently, the frequency-modulated optical pulse leads to a time-varying speckle field that averages out. SSD is routinely used at facilities such as the National Ignition Facility (NIF)[1] and the OMEGA Laser System.[8] The required amount of smoothing and the architecture of the laser systems determine the implementation of SSD: the NIF uses one-dimensional (1-D) SSD with modulation at ~17 GHz and a single diffraction grating in the front end, while OMEGA uses two-dimensional (2-D) SSD with modulation along two axes at ~3 GHz and 10 GHz and multiple gratings.[9] Phase modulation is also required in large-scale, high-energy laser systems to prevent stimulated Brillouin scattering (SBS): a high-intensity monochromatic beam can create acoustic waves in a physical medium (e.g., a fused-silica lens) that will scatter the beam, resulting in instability, losses, and optical damage.[10] Phase modulation generates sidebands that are individually below the threshold for SBS, suppressing its detrimental effect. This modulation is typically performed at a frequency of 3 GHz with a modulation index of ~5 rad on the NIF, resulting in approximately ten sidebands in an ~30-GHz bandwidth.

The NIF is currently configured for indirect drive, where the UV laser beams are incident on the internal sides of a gold hohlraum and generate x-ray radiation that compresses the target. SSD is performed at 17 GHz with a modulation index equal to a few radians. Simulations of direct drive, where the UV beams directly compress the target, on the NIF show that SSD must be implemented on the initial part of the pulse shape with three distinct modulation frequencies (multi-FM).[11] These modulations are approximately at 21.2 GHz, 22.8 GHz, and 31.9 GHz, i.e., at significantly higher frequencies than what is currently being used on existing laser systems for SSD and SBS suppression (SBSS). The main part of the pulse shape, which produces most of the on-target energy, uses SSD at 17 GHz and SBSS. With the parameters of Table 134.V, the multi-FM optical spectrum (98% of the energy in a 200-GHz bandwidth) is ~50% broader than the main-pulse spectrum (98% of the energy in a 133-GHz bandwidth). A fiber front-end prototype demonstrating the required technologies has been developed. It relies on high-bandwidth $LiNbO_3$ phase modulators and Mach–Zehnder modulators for phase modulation and pulse shaping, respectively. Large-scale laser systems operate close to the technological limits of optical components, and amplitude modulation caused by spectral distortion of frequency-modulated signals must be understood and controlled to avoid optical damage. Subsystems that compensate and characterize for frequency-modulation-to-amplitude-modulation (FM-to-AM) conversion have been developed. The front end has supported multiple shot campaigns on the OMEGA EP Laser System[12] to demonstrate the laser and beam-smoothing performance.[13]

In this article, we first describe the architecture of the fiber front end with an emphasis on the modulators used for phase modulation (SSD/SBSS) and amplitude modulation (pulse

Table 134.V: Characteristics of the phase modulations applied in the front end. All the frequencies were multiples of the reference frequency f_{Ref} = 37.998935 MHz. The first two modulations were performed in the main channel; the three other modulations were performed in the picket channel.

Modulation	Frequency (GHz)	Multiple of f_{Ref}	Modulation Index (rad)
Stimulated Brillouin scattering suppression (SBSS)	f_{SBSS} = 3.002	79	5.5
Smoothing by spectral dispersion (SSD)	f_{SSD} = 16.986	447	2.6
Multi-FM 1	f_1 = 21.165	557	0.45
Multi-FM 2	f_2 = 22.837	601	1.04
Multi-FM 3	f_3 = 31.881	839	2.07

shaping) and the subsystems developed to reduce FM-to-AM conversion and safely operate the laser system. The experimental characterization of the fiber front-end performance is then presented, in particular, phase modulation, pulse shaping, and amplitude noise, followed by the conclusions.

Front-End Architecture

1. Requirements

The front-end requirements for this demonstration on the OMEGA EP Laser System have been set based on simulations of polar-drive ignition on the NIF and the requirement that the new front end be integrated into the existing laser systems. The typical pulse shape in the ultraviolet (UV), i.e., after amplification in the full laser system and frequency conversion, is shown in Fig. 134.22. It is composed of two sections:

- Between 0 and 4.5 ns, three short pulses (named "pickets") launch shocks into the target.[14] Each picket has a duration of a few hundred picoseconds and must be phase modulated at three noncommensurate microwave frequencies (multi-FM modulation) to provide optimal beam smoothing on target. The three modulation frequencies in this design are approximately 21.2 GHz, 22.8 GHz, and 31.9 GHz (Table 134.V).

- After 4.5 ns, a rectangular high-energy pulse preceded by a low-intensity step pulse between 4.5 ns and 6 ns is required. The step pulse launches an additional shock into the target before compression by the main high-energy pulse. The main pulse lasts for several nanoseconds but has rise/fall times that are in the hundreds-of-picoseconds range. This pulse must be phase modulated at 3 GHz for SBSS and at 17 GHz for SSD (Table 134.V).

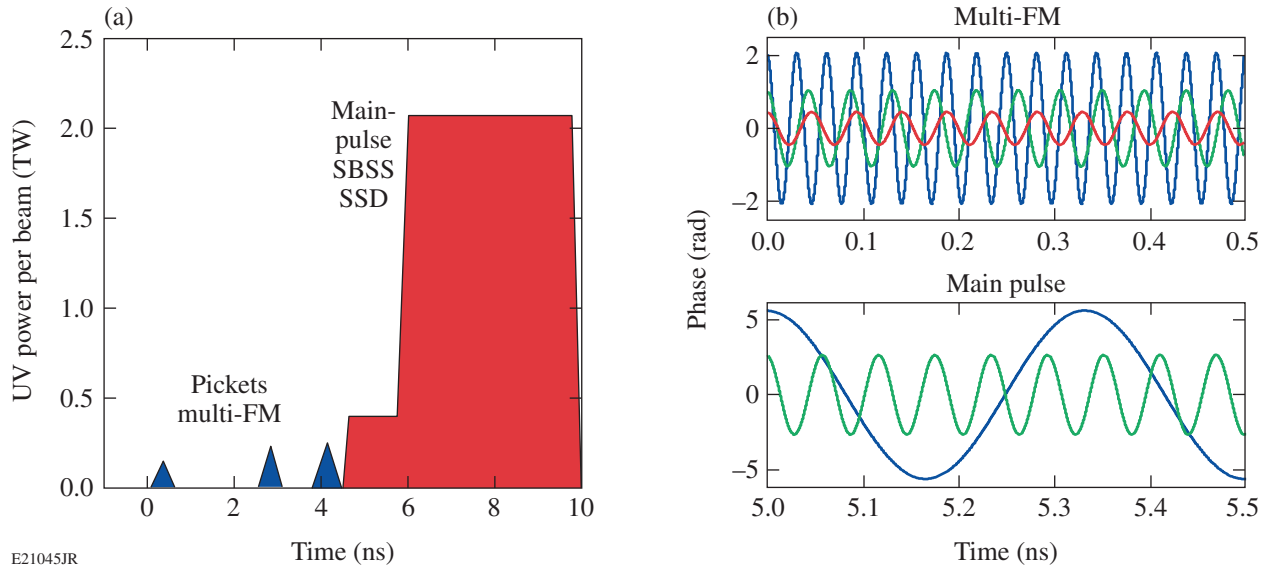

Figure 134.22

(a) Schematic of the pulse shape (power versus time) after frequency conversion at the end of the laser system, composed of three short, low-energy pickets and a main high-energy pulse. (b) Plots of the phase modulations required at the fundamental wavelength on the pickets (f_1, f_2, f_3) and on the main pulse (f_{SSD} and f_{SBSS}), with parameters given in Table 134.V. FM: frequency modulation; SBSS: stimulated Brillouin scattering suppression; SSD: smoothing by spectral dispersion.

The front end must operate at ~1053 nm, which is the peak of the gain for neodymium-doped phosphate glass. It is designed as a proof-of-concept of a system that could be used in the NIF Master Oscillator Room[15,16] and has been built around technologies that are either compatible with its environment and requirements or can be upgraded to suitable technologies for an actual deployment. It must contain fail-safe systems that will interrupt the amplification so that no high-energy pulse propagates in the laser system if such propagation could lead to damage. The output pulses must have low variations in energy and pulse shape, and have sufficient energy to seed the preamplifier module (PAM), a sequence of amplifiers used on the NIF to boost the energy before amplification in the main beamline.[17]

2. General Structure

The front end optically combines two distinct optical channels operating at wavelengths close to 1053 nm—one generating the main pulse and one generating the pickets (Fig. 134.23). The two channels have a symmetric architecture, combining programmable pulse shaping by $LiNbO_3$ Mach–Zehnder modulators driven by arbitrary waveform generators (AWG's), phase modulation by $LiNbO_3$ phase modulators, and two stages of amplification to compensate for propagation and insertion losses. Fail-safe systems protecting the high-energy beamline and components operate in real-time and can interrupt the propagation of an improperly modulated pulse before amplification to high-energy levels. The two channels are combined by a fiber coupler with a fixed coupling ratio. The relative level of the two channels is adjusted via the gain of fiber amplifiers (there are two amplifiers in each channel and one amplifier in the combined section of the front end). Most pulse shapes of interest require similar output levels for the two channels, which is facilitated by the symmetric structure. All components are fiber coupled up to the PAM.

Birefringent optical fibers maintain the polarization state throughout the system. Most components use polarization-maintaining (PM) fibers that support two orthogonal propagation modes. The fibers connecting components and chassis are polarizing (PZ) fibers that support only one propagation mode at 1053 nm: linearly polarized light launched along the guiding direction is nominally transmitted without loss but light polarized along the orthogonal direction is strongly attenuated. The absence of crosstalk in such fibers helps to reduce the FM-to-AM conversion caused by delayed self-interference when successive PM fibers are used.[18] An extinction ratio (ratio of the guided-mode transmission to the blocked-mode transmission) higher than 30 dB is nominally obtained with 4-m patchcords.

The phase-modulation drive voltages are synchronized to the reference frequency $f_{Ref} = 37.998935$ MHz used throughout the OMEGA EP Laser System. The phase modulations at the required five microwave frequencies (Table 134.V) are obtained using commercial phase-locked oscillators, ensuring that the output frequency is an exact integer multiple of the reference frequency. A phase shifter on each phase-modulation drive allows for independent temporal tuning of the phase modulation relative to the optical pulse. The performance of on-target smoothing does not depend significantly on the relative phases of the three sinusoidal modulations.[11] Tuning of the relative phases is included because it could be used to control the amplitude of the power modulation caused by FM-to-AM conversion, although this has not been studied in detail. All

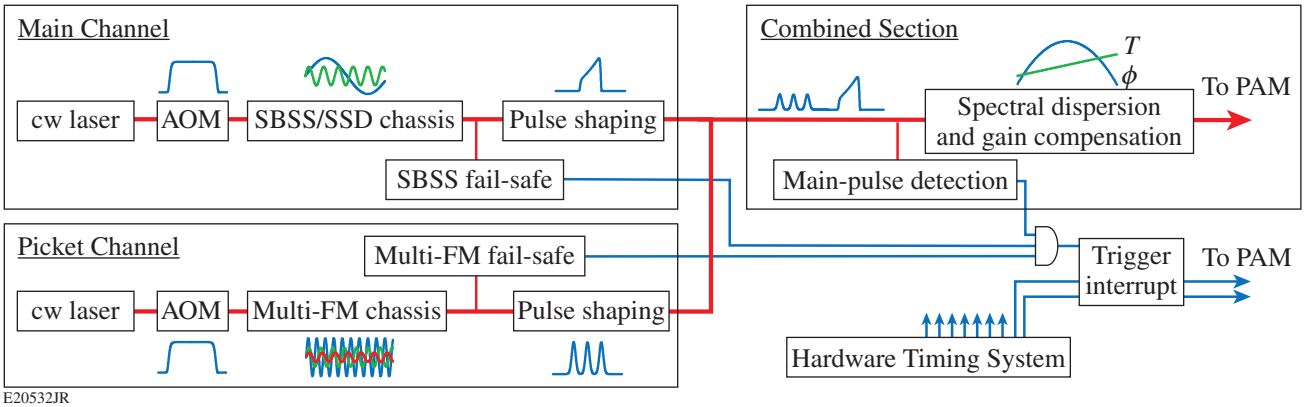

Figure 134.23

General layout of the front end. The picket and main channel are independently phase modulated and shaped after gating of a continuous-wave (cw) seed source by an acousto-optic modulator (AOM). Dispersion and amplitude compensations are performed after optical combination. Three fail-safe systems are used to ensure safe operation. Five fiber amplifiers (two in each independent section and one in the combined section) have not been represented. PAM: preamplifier module.

components in the front end are synchronized to the Hardware Timing System (HTS) used throughout the laser facility, which is also synchronized to f_{Ref}. The fiber front end operates at 300 Hz. All electronic components (including the fail-safe systems described in the following subsections) can operate at 960 Hz, the repetition rate of the NIF front end. The ytterbium-doped fiber amplifiers have not been tested at 960 Hz, which corresponds to operation close to the fluorescence lifetime of ytterbium, but similar amplifiers are operated in the NIF front end at that rate. The timing of the two channels relative to each other and to the laser facility is adjusted by controlling the delay of all the corresponding trigger signals from the HTS.

3. Main Channel

The main channel (Fig. 134.23) uses a cw (continuous-wave) laser operating at ~1053 nm gated by an acousto-optic modulator (AOM) to a duration of 100 ns. The gated pulse is phase modulated by the custom three-section phase modulator shown in Fig. 134.24. The phase modulator has three consecutive sections of $LiNbO_3$ that can be independently driven. Each section is externally terminated to allow for the use of high-power drives that could damage an internal 50-Ω termination. A single device with three phase-modulation sections is advantageous compared to the cascaded sequence of three distinct phase modulators: the modulator is more compact and easier to mount, and the optical losses from input to output are lower than 5 dB. In the main channel, phase modulation is provided in only two of the three sections. In one section, phase modulation at 3 GHz is induced with a modulation index of 5.5 rad for SBSS. In the second section, phase modulation at 17 GHz with an index of 2.6 rad is performed for on-target beam smoothing. The resulting optical spectrum is plotted in Fig. 134.25(a).

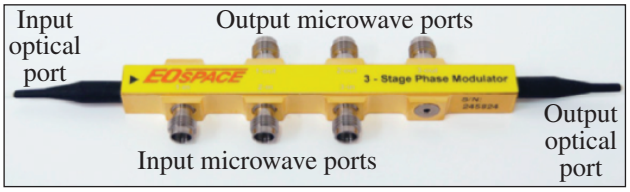

Figure 134.24
The three-section phase modulator, with distinct input and output ports for the three phase-modulating sections.

Pulse shaping is implemented in a custom two-section modulator comprised of two consecutive $LiNbO_3$ Mach–Zehnder modulators (MZM's). One of the MZM's is driven by a shaped voltage from the amplified output of a 10-GS/s AWG

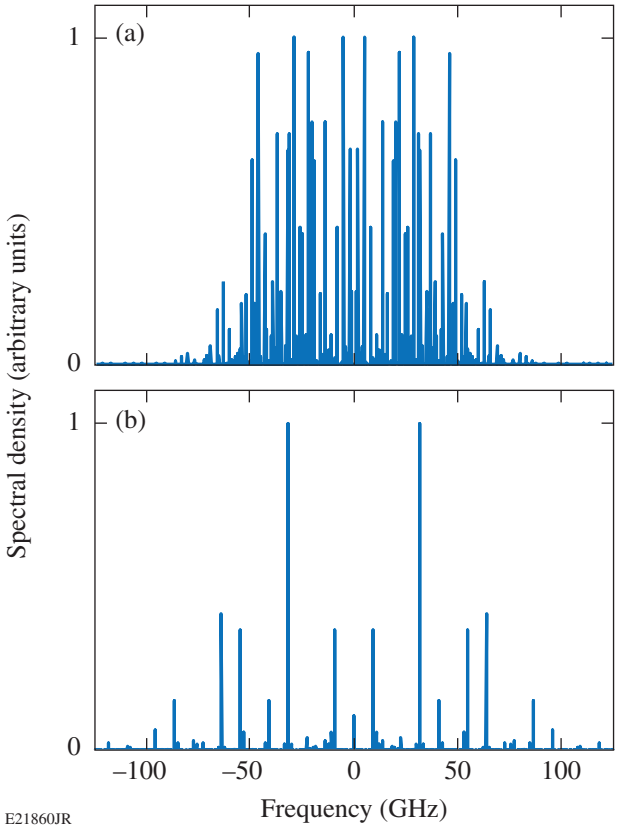

Figure 134.25
(a) Optical spectrum of the pulse after phase modulation in the main channel; (b) optical spectrum of the pulse after phase modulation in the picket channel.

(Kentech AWG-10). This modulator is used for precise pulse shaping, ensuring that the channel output meets the requirements imposed by the target physics and the safety of the laser system. The other MZM is driven by an unshaped square pulse with programmable duration. This MZM acts as a gate on the shaped pulse: when the duration of the square pulse is set appropriately, the modulator does not shape the optical pulse but enhances the temporal contrast (ratio of the power at full transmission to the power at extinction). For example, with two MZM's having a nominal extinction ratio of ≥20 dB, the overall extinction ratio is ≥40 dB. High extinction ratios are particularly important when optically combining optical pulses from two distinct sources because leakage from one source can detrimentally interfere with the pulse from the other source.

A fraction of the main channel is sent to a fail-safe system to monitor the 3-GHz phase modulation and avoid optical damage from SBS.[10] The SBSS fail-safe is a unit provided by Lawrence Livermore National Laboratory.[15] The unit intentionally induces FM-to-AM conversion on the monitored signal with a spectral filter to convert the 3-GHz phase modulation into a

3-GHz amplitude modulation that can be measured with an AM detector. The unit monitors in real-time the phase-modulation amplitude and duration on the optical pulse, i.e., it ensures that the phase modulation is sufficient and applied during the total length of the ~100-ns pulse gated by the AOM. It also detects undesirable characteristics of the optical pulse, spurious amplitude modulation not intentionally generated by the fail-safe system, and sudden changes in the input energy that could prevent the fail-safe from adequately detecting a fault. Its output is a 5-V logic trigger that is high if the duration and amplitude of the phase modulation are nominal and low if at least one of the safe operating conditions is not met. This trigger is sent to the PAM Trigger Interrupt Safety System (PTISS) to prevent unsafe high-energy amplification if there is a fault.

4. Picket Channel

The picket channel (Fig. 134.23) uses a set of optical components identical to the one deployed on the main channel. The three sections of the phase modulator are driven by the three distinct phase modulations at 21.2 GHz, 22.8 GHz, and 31.9 GHz with respective modulation indices of 0.45 rad, 1.04 rad, and 2.07 rad. The resulting optical spectrum is plotted in Fig. 134.25(b). Pulse shaping is performed by driving one section of a two-section MZM with the output of a Tektronix 7122 AWG operating at 24 GS/s amplified by a broadband amplifier. The other section is driven by a square pulse to increase the extinction ratio.

The pickets are nominally short optical pulses, i.e., with a spectrum relatively broad compared to the typical nanosecond pulses shot on high-energy laser systems, therefore reducing concern for SBS in the absence of phase modulation, but a fail-safe system was designed to prevent high-energy amplification in the absence of significant phase modulation on this channel. The fail-safe system measures the power in two spectral bands of the phase-modulated pulse, one on each side of the carrier frequency, to infer the amount of phase modulation. A diffraction grating disperses the optical pulse, and a focusing lens generates a Fourier plane in which spectral components are spatially separated and individually focused. Multimode optical fibers mounted on a V-groove array are used at the Fourier plane to couple light from the two bands of the optical spectrum to two amplified photodiodes. The system is designed to detect the optical power in two bands centered 127.6 GHz apart, i.e., on the sidebands of the carrier at twice the modulation frequency f_3. These two bands correspond to the spectrally dispersed light from the diffraction gratings on two fibers separated by 500 μm at the Fourier plane. Each 105-μm-diam fiber integrates the optical power over 26.8 GHz. Thresholds for the measured powers are set when the system operates at the default phase-modulation amplitudes so that the fail-safe trips when the modulation at f_3 does not have sufficient amplitude, regardless of the presence of the modulation at f_1 and f_2. This would detect malfunction of the entire phase-modulation unit for the picket channel and malfunction of the sub-unit responsible for phase modulation at the frequency f_3. A precise analysis of the different failure modes and their impact on SBS has not been conducted at this point, but operation with f_3 operating at its nominal modulation index was thought to be safe for the system because the corresponding spectrum is spread over more than 100 GHz with each sideband broadened to several GHz because of the short picket duration. Simultaneous failure of the two sub-units responsible for phase modulation at f_1 and f_2 is highly unlikely because of the architecture of the phase-modulation unit; therefore, the detection of the frequency f_3 indicates that at least one other modulation frequency is also present, further contributing to SBS reduction. The fail-safe 5-V logic output (high for the nominal modulation and low for insufficient bandwidth) is sent to the PTISS to prevent high-energy amplification in the latter case.

5. Combined Section

The picket and main channels are combined with identical polarization states by a fiber coupler after timing and amplitude adjustments. Chromatic dispersion and nonuniform spectral gain are compensated identically after the combiner for economy of scale and minimized complexity. A rack-mounted device combining dispersion and amplitude compensation has been built (Fig. 134.26). Spectral distortion (i.e., phase and/or amplitude) of a phase-modulated pulse leads to amplitude modulation in the time domain. FM-to-AM conversion is detrimental to the operation of high-energy laser systems because amplitude modulation leads to higher peak power for a given pulse energy.[19,20] Amplitude modulations are also a concern when the propagation is nonlinear. The chromatic dispersion of optical fibers and other optical components at 1053 nm corresponds to a positive second-order dispersion ($d^2\varphi/d\omega^2 > 0$, where φ is the phase accumulated by propagation as a function of frequency). The total length of fiber for each channel (calculated from the output of the phase modulator to the last fiber amplifier) is ~130 m. A frequency-dependent amplitude modulation arises from gain tilt in the ytterbium-doped fiber amplifiers and the Nd:glass regenerative amplifier. The fiber amplifiers are broadband, but their gain varies over the spectral range of interest, with a typical gain slope of 5% per 100 GHz (i.e., the difference between the gain at f_0 + 50 GHz and f_0 – 50 GHz normalized to the gain at f_0 is 5%). The regenerative amplifier gain is approximately Gaussian with a

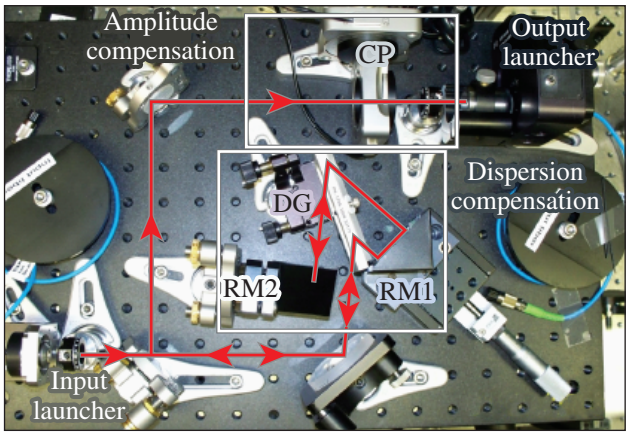

Figure 134.26
The amplitude/dispersion compensator. The dispersion compensator is composed of two roof mirrors, for horizontal (RM1) and vertical (RM2) beam displacement and inversion, and a transmission diffraction grating (DG). The amplitude compensator is composed of a calcite plate (CP) mounted on two rotation stages.

full width at half maximum (FWHM) of 400 GHz. The front end is configured to seed the regenerative amplifier on the long-wavelength slope of the Gaussian gain curve, for which the gain slope is approximately 40% per 100 GHz. The uncompensated gain slope over the fiber front end and regenerative amplifier would lead to large-amplitude modulation. Spectral distortions have been compensated with fiber-coupled free-space subsystems that were combined in a single enclosure to minimize losses: without any spectral amplitude modulation, the input-to-output loss is ~5 dB.

Dispersion compensation ($d^2\varphi/d\omega^2 < 0$) is performed with a compact compressor using a single transmission grating in a four-pass configuration. The transmission grating is a 1700-l/mm fused-silica grating used in the Littrow configuration. The diffracted beam is sent back to the same grating after a lateral displacement and horizontal beam inversion by a roof mirror; it is then diffracted again by the grating, displaced vertically by another roof mirror, and sent back to the grating, first roof mirror, and grating. The dispersion is controlled by a translation stage on the first roof mirror modifying the distance between the first and second diffractions on the grating and identically between the third and fourth diffractions. The compensator was designed to overcompensate the dispersion of the front end because of its future use in a system mimicking the front end of the NIF. In that system, the front end is in a different room from the NIF PAM's, resulting in the shaped phase-modulated optical pulse traveling in several hundred meters of PZ fibers. This compensator is built for ~100 m of additional PZ fiber between the front end and the PAM, even if these two systems are physically separated by only a few meters in our system. Translation of the first roof mirror allows for an increase in the magnitude of the introduced negative second-order dispersion to compensate for longer fiber lengths.

The optical source is linearly polarized, allowing for spectral amplitude modulation using a Lyot-type filter implemented with a birefringent calcite plate.[21] The plate can be rotated relative to a vertical rotation axis (Axis 1) and relative to an axis perpendicular to its surface (Axis 2) to adjust the spectral modulation. At normal incidence, rotation around Axis 2 changes the relative ratio of the two polarization components traveling along the two axes of the plate, which controls the depth of the spectral modulation. Rotation around Axis 1 changes the retardance of the plate, which controls the location of the spectral modulation along the frequency axis. The calcite plate is followed by a zeroth-order half-wave plate and a PZ fiber acting as a polarizer. Calcite plates with thicknesses from 1 mm to 4 mm have been used during a testing phase, with similar results, and a 4-mm calcite plate has been installed for operation.

The pickets are nominally short pulses that can reach high peak powers if the system is configured for the generation of a high-energy main pulse but the latter pulse is absent—for example, because of an equipment failure, triggering issue, or operator error. A fail-safe system ("main-pulse detection fail-safe") prevents amplification and subsequent damage when the main pulse is absent. This system uses photodetection and integration of the combined output to generate a signal representative of the front-end output energy, which must be higher than a user-set threshold for safe operation. The system output is a 5-V logic signal that is high when operation is safe and low otherwise. This signal is sent to the PTISS.

The three fail-safe systems (SBSS fail-safe operating on the main channel; picket-bandwidth fail-safe operating on the picket channel; and main-pulse detection fail-safe operating on the combined output) provide three logical signals to the PTISS. The latter system is fed with two triggers: the switch-out trigger to the Pockels cell in the regenerative amplifier and the slicer-on trigger for the Pockels cell located after the regenerative amplifier. In safe operation, the front end delivers a seed pulse to the regenerative amplifier; this pulse is amplified after multiple round-trips in the cavity; the amplified pulse is ejected by the Pockels cell located inside the amplifier; and the output pulse is gated by an external Pockels cell (the slicer) that is turned on to let the ejected pulse go through. In the absence

of trigger signals from the three fail-safe systems, the PTISS interrupts the two triggers. The pulse being amplified in the regenerative amplifier remains in the laser cavity and is not ejected by the intracavity Pockels cell. The slicer is not turned on, further decreasing the transmission.

Front-End Performance

1. Pulse Shaping

Temporal characterization of the shaped optical pulses was performed with a 45-GHz, 120-GS/s Teledyne LeCroy Wavemaster oscilloscope and a fiber-coupled 60-GHz Discovery Semiconductors DSC10 InGaAs photodetector. The impulse response of this diagnostic had a FWHM lower than 20 ps. Various algorithms and procedures were tested to correct the frequency-dependent response of the photodetection system (for example, isolating one frequency component and adjusting its spectral amplitude by the known spectral response at that particular frequency to compare its amplitude to a prediction made using known system parameters). It was decided to not use post-processing of the measured waveforms when reporting amplitude noise, although the reported noise values correspond to averages of the noise values over multiple waveforms, as described below. Most measurements have been performed in the front end at 300 Hz and after the regenerative amplifier since that amplifier has the largest amount of square-pulse distortion in our demonstration (the gain on the pulse is a decreasing function of the time because the leading edge of the pulse propagates in the amplifying medium before the trailing edge and experiences more gain). It also has the most-significant impact on the optical spectrum because of its relatively narrow amplification bandwidth and large gain slope. Finally, it operates at a repetition rate of 1 Hz, allowing for the acquisition of statistically meaningful sets of data: the rod amplifier in the PAM after the regenerative amplifier typically operates at one shot every 20 min, significantly impacting the experimental ability to collect multiple data sets for statistical analysis.

The impulse response of the picket and main pulse-shaping systems has been determined by setting one electrical sample of the corresponding AWG to full voltage and measuring the optical output as a function of time. The measured responses have a FWHM of 55 ps and 115 ps for the picket channel and main channel, respectively. The corresponding 10/90 rise and fall times, measured on the impulse responses, are similar to the FWHM for the two systems. These values correspond to to the pulses shaped by the fiber front end. Because of the pulse-front tilt introduced by the SSD grating (~230 ps across the full beam), the on-target pulse duration is significantly longer. The choice of the faster AWG for the picket channel stems from the technical requirements for pulse shaping in these two channels, although generating pickets shorter than ~100 ps is not required.

A wide range of pulse shapes has been generated with the two channels, including single and multiple pickets, long square pulses, and shaped pulses. Figure 134.27(a) displays an example of a pulse shape with three pickets and a long shaped pulse measured at the output of the regenerative amplifier. Figures 134.27(b) and 134.27(c) show close-ups of the measured pulse shape with shaded areas, indicating the root-mean-square (rms) and peak-to-valley variations at each acquisition time, obtained by measuring 50 successive pulses. The rms and peak-to-valley energy variations over 50 measurements are 1.9% and

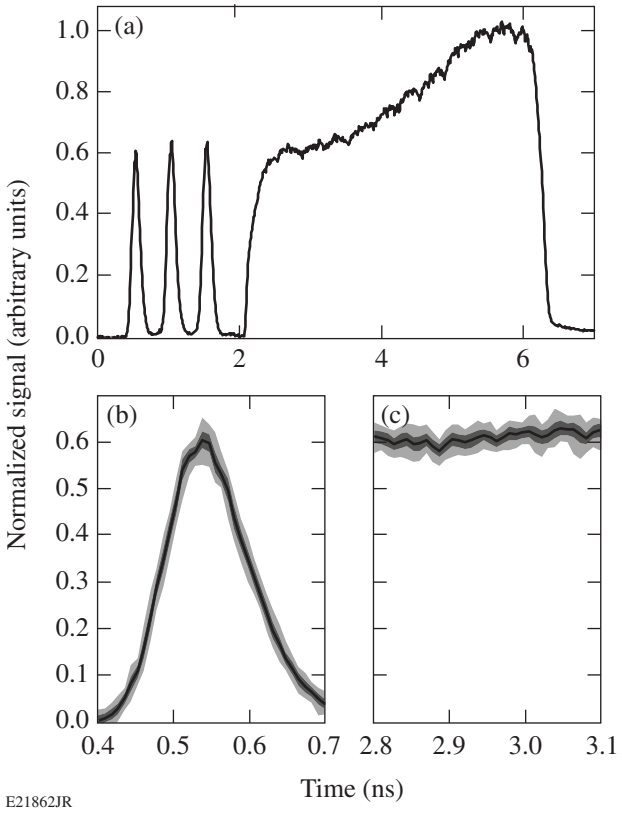

Figure 134.27

(a) Example of pulse shape $P(t)$ measured at the output of the regenerative amplifier. The plotted pulse is an average of 50 successive measurements. [(b) and (c)] Close-ups of the first picket (time between 0.4 and 0.7 ns) and the main pulse (time between 2.8 and 3.1 ns). The black line corresponds to the average of 50 measurements; the dark-gray–shaded region corresponds to the power range $[P(t)-\sigma(t), P(t)+\sigma(t)]$, where $\sigma(t)$ is the standard deviation of P at time t over the 50 measurements, and the light-gray–shaded region corresponds to the power range $[M_-(t), M_+(t)]$, where $M_-(t)$ and $M_+(t)$ correspond to the lowest and highest value of the power measured at time t over the 50 measurements.

9.8%, respectively, for one picket and 1.2% and 5.1%, respectively, for the main pulse. These are overestimates of the actual energy variations because of the oscilloscope analog-to-digital conversion noise, particularly for the picket with a FWHM of ~100 ps for which the energy is obtained by summation over a small number of acquired samples. A 1-ns pulse generated by the picket channel in the same conditions has rms and peak-to-valley energy variations equal to 1.8% and 6.6%, respectively, while the energy variations calculated in a 1-ns window for the monochromatic laser chopped by the AOM before phase modulation are 0.5% and 2.0%. The energy statistics are in agreement with the energy statistics independently measured with an energy meter that indicates a rms variation lower than 2% after the regenerative amplifier seeded by either channel.

The jitter and timing drift between the two channels have been measured over 300 waveforms produced by the front end acquired in a short time window (1.5 min) or long time window (150 min) by estimating the location of the 50% points of the picket-channel trailing edge and main-channel leading edge. The relative timing between the two channels has a rms jitter of 15 ps and a monotonic drift of 20 ps over 2.5 h. The timing drift is attributed to drifts in the pulse-shaping electronics (e.g., triggers) and small temperature changes (although the front end operates in a temperature-controlled environment, each channel contains more than 100 m of optical fibers that are physically distinct). The timing of the picket channel and main channel relative to the oscilloscope time base has rms jitter values of 13 ps and 9 ps, respectively. These are overestimates of the jitter of the front end relative to the reference frequency, i.e., the remainder of the laser system, since they include the oscilloscope jitter. These values are within the required range for this demonstration. The jitter and the finite rise and fall times of the shaped pulses constrain the relative timing between the channels to values greater than 125 ps (delay between the 50% points of the picket-channel trailing edge and main-channel leading edge). Random amplitude modulation related to interference of the two optical pulses is observed for shorter separations.

2. Phase Modulation

Precise characterization of the phase modulators and resulting phase modulation is important. The modulators must first be characterized to ensure that they are suitable for this application, i.e., that they can be driven adequately at the five different microwave frequencies with the required modulation index. During operation, the phase-modulation index must be characterized to ensure that it matches the required specifications. A cw laser field at the optical frequency f_0 phase modulated at the frequency f_m with modulation index m has the temporal electric field

$$E(t) = E_0 \exp(2\pi i f_0 t) \exp[im \sin(2\pi f_m t)]. \quad (1)$$

In the frequency domain, the field is given by

$$\tilde{E}(f) = \sum_n J_n(m)\,\delta(f - f_0 - n f_m), \quad (2)$$

where J_n is the Bessel function of the first kind of index n. The optical spectrum is composed of an infinite number of sidebands at the frequencies $f_0 + nf_m$ with spectral density $|J_n(m)|^2$, but 98% of the energy is concentrated in a $2mf_m$ bandwidth centered at f_0 according to Carson's rule.

Fitting the measured spectrum with the calculated spectrum of a phase-modulated field, where m is the single parameter, makes use of all the measured data and is computationally efficient; this was chosen for modulation-index determination at frequencies corresponding to sidebands that can be resolved. The spectral modes corresponding to f_{SSD} = 17 GHz, f_1 = 21.2 GHz, f_2 = 22.8 GHz, and f_3 = 31.9 GHz are easily resolved with a commercial scanning grating monochromator. The modes corresponding to 3 GHz cannot be individually resolved because the response of the monochromator broadens the individual spectral modes, resulting in a smoothed spectrum. One experimental solution is to develop a dedicated diagnostic measuring the optical spectrum with a resolution suitable to resolve spectral modes separated by 3 GHz (typically sub-GHz); for example, using a scanning Fabry–Perot etalon. It was chosen to use numerical post-processing to estimate the modulation index in this case.

For modulator characterization, a microwave signal generator was used to generate drives with frequency ranging from 15 GHz to 40 GHz. The power of the drive was calibrated at each modulation frequency. The modulation index was determined for each of the three sections of the phase modulators. The corresponding V_π was calculated by scaling the phase-versus-voltage measurement, where the phase is related to the modulation index and the voltage is proportional to the square root of the power. The characterization of the V_π is shown in Fig. 134.28 for one of the modulators. The three sections behave similarly, and the V_π increases from ~5 V to ~7 V in the measurement range. V_π values lower than 7 V are acceptable since the voltages required to reach the requested modulation indices are within the range of medium-power solid-state microwave amplifiers. Similar performance was measured on three other phase modulators.

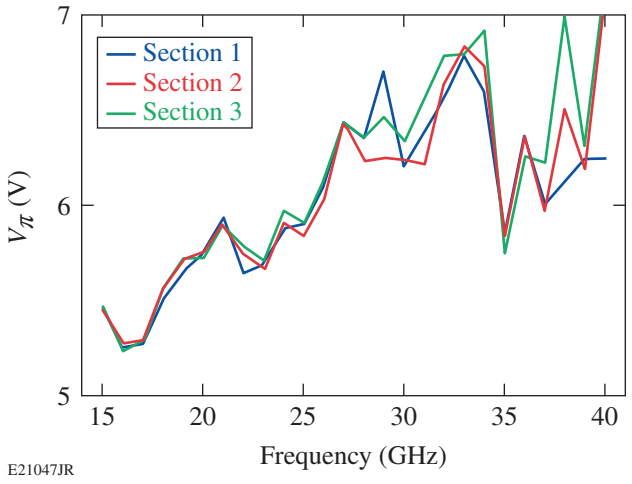

Figure 134.28
Determination of V_π on the three sections of a phase modulator.

For operational characterization of the frequency modulation induced by one modulator, the other drive voltage(s) is (are) turned off, e.g., the drives at f_1 and f_2 are turned off when characterizing the modulation at f_3. An optical spectrum is measured and fitted to determine the modulation index. The drive voltage is increased or decreased via a continuous attenuator, and the measurement is repeated until the measured index matches the requested index within an acceptable uncertainty. Figure 134.29(a) shows the agreement between the measured spectral modes at frequency f_3 with the modes obtained after fitting. Figure 134.29(b) shows the measured optical spectrum when the three drives to the picket-channel phase modulator are turned on. This spectrum agrees very well with the calculated spectrum. For operational characterization of the modulation index at f_{SBSS}, which leads to spectral modes that cannot be distinguished with the available monochromator, an indirect approach was used. The archived spectrum of a cw source, e.g., the spectrum of the same source with all modulations turned off, was used as the instrument response to calculate the optical spectrum that should be measured for a given modulation index. Figure 134.30(a) shows that the bandwidth of the convolved spectrum increases monotonously with the modulation index and is within 1 GHz of the actual bandwidth for modulation indices between 5 and 6 rad. The drive for f_{SSD} is turned off and the modulated spectrum with f_{SBSS} turned on is measured. The modulation drive is precisely set by comparing the measured bandwidth to the bandwidth of the theoretical spectrum corresponding to 5.5 rad convolved with the measured response function. The theoretical spectrum, measured response function, and convolved spectrum are shown in Fig. 134.30(b). The excellent agreement between the measured and convolved spectrum, demonstrated in Fig. 134.30(c), and the monotomic relation between actual bandwidth and measured bandwidth, demonstrated in Fig. 134.30(a), allow us to conclude that the modulation index is adequately set.

3. Extinction of Mach–Zehnder Modulators

MZM extinction is a critical parameter of the pulse-shaping systems because interference between the co-polarized optical waveforms after combination of the picket and main channel can generate large amounts of amplitude modulation. The combined field from the two pulse-shaping channels is

$$p(t) = p_1(t) + b_1(t) + p_2(t) + b_2(t), \tag{3}$$

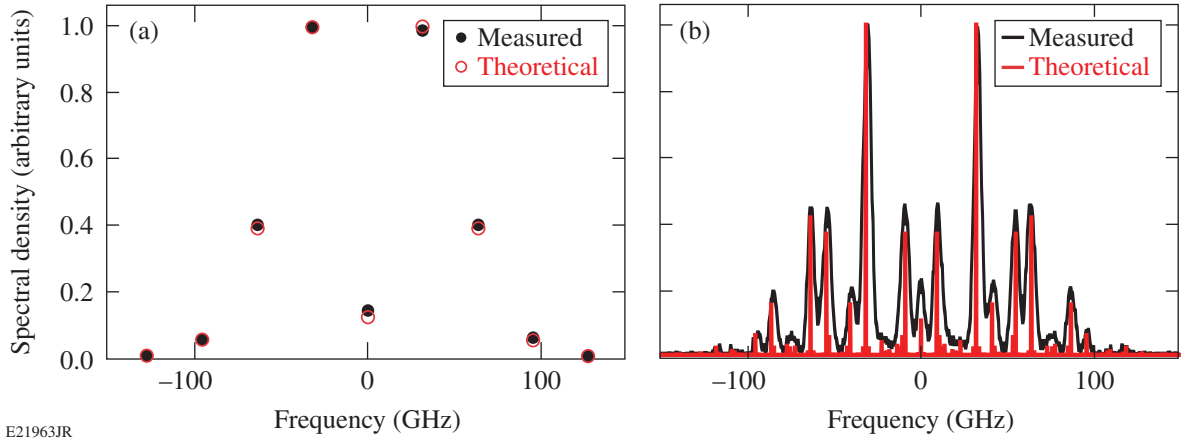

Figure 134.29
(a) Example of a measured spectrum (solid black circles) and fit (open red circles) for the modulation frequency f_3, (b) measured and theoretical optical spectra when the three multi-FM drives are turned on.

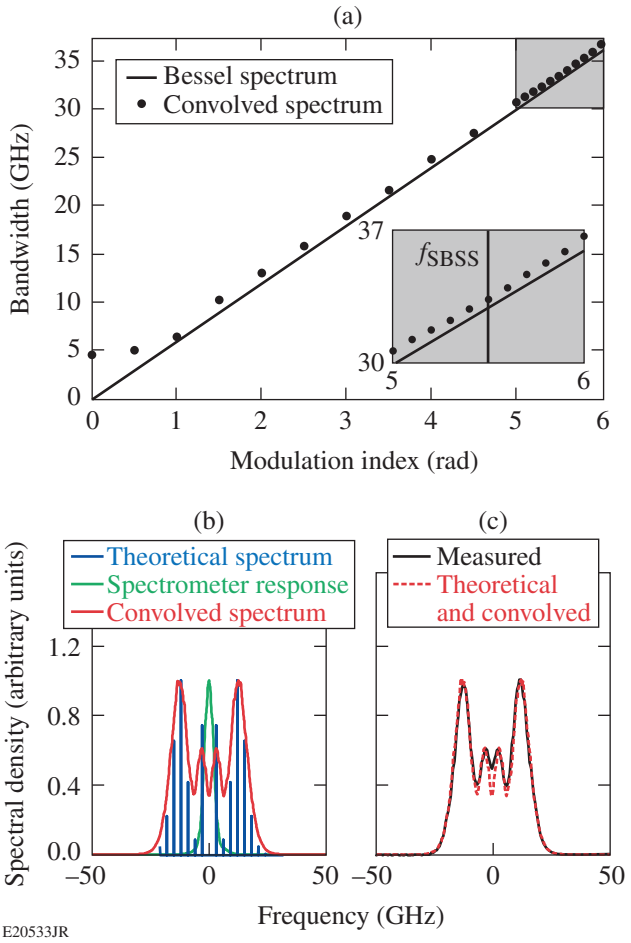

Figure 134.30

(a) Plot of the FWHM of the spectrum obtained by convolution of the measured monochromator response with the theoretical spectrum of a monochromatic source after phase modulation at f_{SBSS}. The inset shows a close-up of the range of modulation index between 5 and 6 rad. (b) Theoretical spectrum of a phase-modulated field at 3 GHz with a modulation index of 5.5 rad, measured response function of the spectrometer, and spectrum obtained by convolution of these two spectra. (c) Comparison of the measured spectrum with the convolved spectrum calculated with the nominal SBSS specifications.

where p_1 and p_2 are the fields of the two shaped pulses, b_1 is the field leakage of channel 1, and b_2 is the field leakage of channel 2. p_1 and p_2 are finite-duration pulses that are not overlapping because the two channels are timed to generate distinct pulse shapes; p_1 and p_2 are equal to zero during b_1 and b_2, respectively. With these definitions, the power is

$$P(t) = P_1(t) + P_2(t) + 2\mathrm{Re}\left[p_1(t)b_2^*(t)\right] + 2\mathrm{Re}\left[p_2(t)b_1^*(t)\right] + 2\mathrm{Re}\left[b_1(t)b_2^*(t)\right] + B_1(t) + B_2(t), \quad (4)$$

where P_1 and P_2 are the shaped pulses of interest, $p_1 b_2^*$ and $p_2 b_1^*$ are the interference of each shaped pulse with the background leakage from the other channel (the main source of noise), and the other terms correspond to the power and interference of the backgrounds (usually negligible). A channel with extinction ratio R leads to a modulation with peak-to-valley amplitude equal to $4\sqrt{R}$ at times when the pulse generated by the other channel has a power equal to 1. This modulation can be highly detrimental: for $R = 20$ dB, the resulting noise is 40%, and increasing R to 40 dB decreases the peak-to-valley noise to 4%, still negatively impacting the system performance. If the same monochromatic laser is used in the two channels, the self-interference will manifest itself as an energy variation from shot to shot, owing to the slow phase drift between the two channels. If two distinct lasers with an optical frequency difference Δf_{12} are used, the interference is a time-varying amplitude modulation of the optical pulse at the frequency Δf_{12}.

The two cascaded MZM's in each channel ensure that the intrinsic extinction ratio is higher than 40 dB, assuming that the corresponding voltage biases are adequately set. The pulse-shaping systems are calibrated for optimal biasing on each MZM. The front end is built with two distinct monochromatic lasers that are spectrally tuned to make the frequency of their interference easily measurable, i.e., distinct from all the microwave frequencies potentially present in the system (all the frequencies in Table 134.V and the sum and differences of all the frequencies present in a given channel), within the bandwidth of the photodetection system (lower than 45 GHz). The frequency of the offset must be small enough that the two channels essentially have the same central wavelength to avoid impacting amplification and frequency conversion to the UV and allow for identical dispersion compensation. The beams corresponding to the two channels are spatially offset in the far field after the SSD grating because of the angular dispersion. The beam corresponding to the broadest spectrum was chosen for alignment because of the more-stringent alignment requirement to avoid spectral clipping by pinholes in the far field. A frequency approximately equal to 5 GHz was chosen. The seed lasers are spectrally tuned by temperature-controlled fiber Bragg gratings with a spectral drift much smaller than 1 GHz over extended periods of time. The frequency offset is quite stable once set. Figure 134.31 shows examples of waveforms measured with proper biasing and with an intentional bias offset. The bias voltage of the two MZM's in each channel is optimized daily by measuring their transmission as a function of the voltage and determining the voltage for minimal transmission. Bias drift caused by charge accumulation is avoided by temporal alternation of the bias between the

optimal value in a time interval encompassing the shaped pulse and another value to set the time-averaged voltage to zero. No interference between channels has been observed with these pulse-shaping systems and procedures and no fail-safe system actively detecting the interference was implemented because of the reliability and stability of this approach, which is also used for pulse shaping on OMEGA[8] and OMEGA EP.[12]

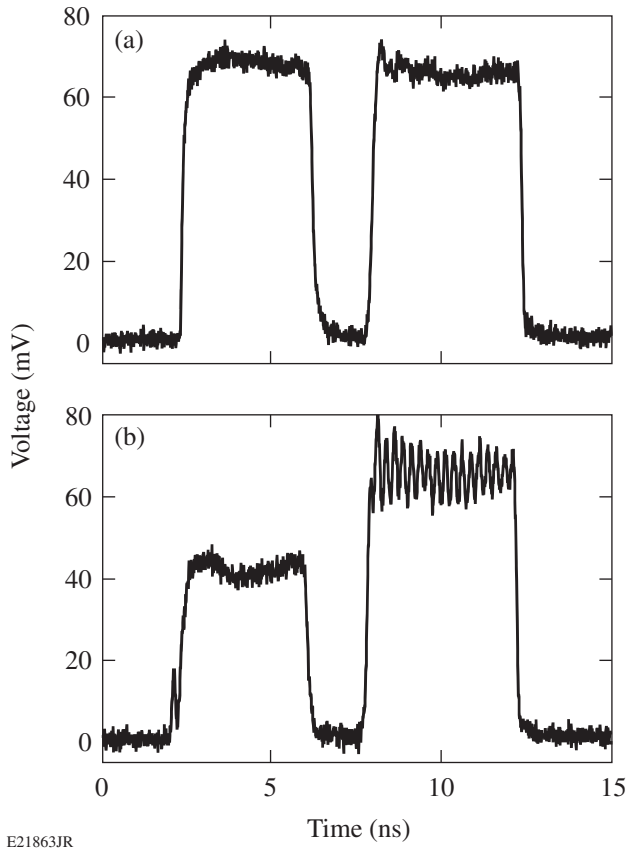

Figure 134.31
Measurement of the pulse shape obtained by combining the picket channel (first pulse) and the main channel (second pulse) in (a) optimal biasing conditions and (b) when the bias of the gate MZM of the picket channel is purposely offset by $\sim V_{\pi}/10$. In the latter case, the amplitude of the first pulse is reduced because of the lower transmission, and AM at ~5 GHz is present on the second pulse because of the increased background.

4. Dispersion Compensation

Dispersion compensation is optimized by first accounting for all sources of chromatic dispersion in the full laser system, from the fiber-coupled phase modulators to the end of the large Nd:glass amplifiers, with optical fibers in the front end being the largest contributor. The two channels in the front end are symmetric, and optimal compensation is expected to be reached for these two systems for the same setting of the dispersion compensator. A 100-m PZ patchcord was initially installed between the front end and the NIF PAM, based on an estimate of the dispersion of the fiber in the front end and the single-grating compressor. Various lengths of PZ fiber were added between the output of the regenerative amplifier and the temporal diagnostic, and the resulting amplitude noise was estimated on a pulse from the picket channel with the three multi-FM modulations turned on (Fig. 134.32). Dispersive propagation has the same effect on the AM whether it occurs before or after the regenerative amplifier in the absence of nonlinearity in that amplifier. Once the optimal fiber length was determined, the corresponding patchcords were placed between the front end and the amplifier to optimize the the amplified signal propagating in the laser system. It is not known if the propagation in the regenerative amplifier is perfectly linear, but no siginificant difference in the measured AM was found when dispersion compensation was adjusted before or after the amplifier.

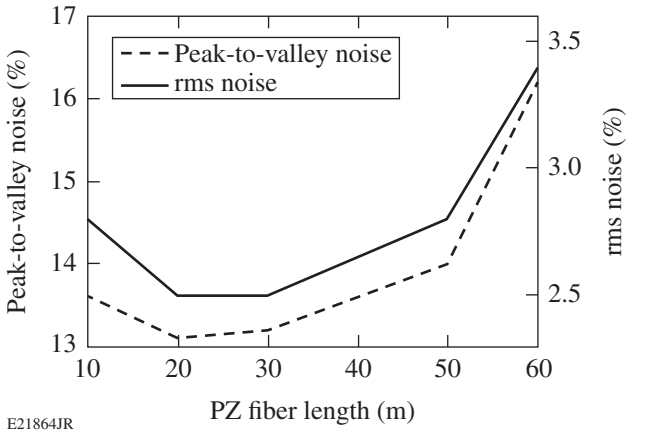

Figure 134.32
Amplitude noise [dashed line: peak-to-valley noise; solid line: rms (root-mean-square) noise] measured as a function of the length of the polarizing (PZ) fiber added before photodetection.

5. Amplitude Compensation

Spectral amplitude compensation is performed by tuning the two angles of the birefringent calcite plate relative to the incident beam. Initial tests and setup used measurements obtained with a spectrometer: the spectrum at the output of the regenerative amplifier is monitored as the plate is tuned by an operator, and the match between the measured spectrum and the expected spectrum (e.g., the spectrum of the pulse with f_1, f_2, and f_3 on) is used as feedback. Figure 134.33 compares the optical spectrum measured after the phase modulator and after the regenerative amplifier. These two optical spectra are indistinguishable and are in excellent agreement with the

theoretical spectrum. Although some amplitude modulation of the spectrum might still be present (beyond the measurement capability in the spectral domain), the time-domain amplitude-noise measurements presented in the next section indicate that the spectral gain tilt in the fiber amplifiers and the regenerative amplifier are adequately compensated. During operation, the amplitude noise measured in the time domain is used as the feedback mechanism. The rf spectrum of the measured waveform (e.g., a square pulse with all multi-FM frequencies turned on at the output of the regenerative amplifier) is calculated in real-time and an operator minimizes the observed rf tones. The amplitude noise on the waveform is then determined. The measured amplitude noise must be below 20% peak-to-valley, as required by a noise budget made for the entire OMEGA EP Laser System. Values of the order of 15% are typical for the peak-to-valley noise, corresponding to rms noise of the order of 3%. The amplitude compensator is stable enough for operation without active stabilization: the amplitude noise was observed over several days without significant increase.

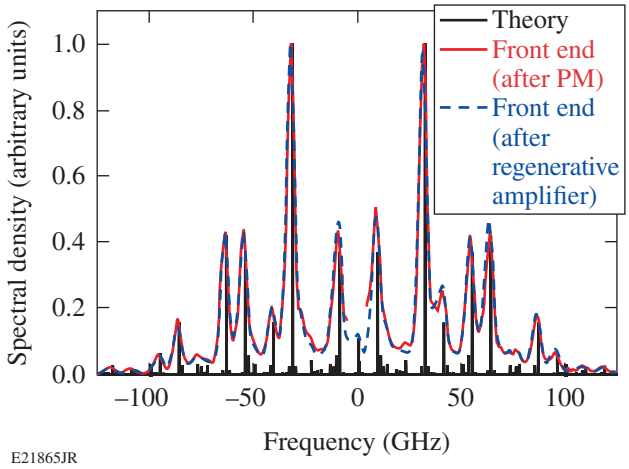

Figure 134.33
Optical spectrum corresponding to a pulse with the three multi-FM frequencies calculated (solid black line), measured after the phase modulator (PM) (solid red line), and measured after the regenerative amplifier (dashed blue line). The measurements were performed with a grating spectrometer having a resolution of 5 GHz. The spectral density data between –5 GHz and +5 GHz after the phase modulator have been removed because the data in that range are corrupted by the cw leakage from the AOM integrated by the detector at the Fourier plane of the spectrometer.

6. Amplitude-Noise Measurements

Amplitude-noise measurements were routinely performed at the output of the regenerative amplifier in the PAM. Quantifying the amplitude noise is crucial for the operation of a large-scale laser system because AM increases the peak power incident on the optical components for a given energy. A power increase can lead to higher nonlinearity experienced by the optical pulse and to optical damage. This amplifier operates at 1 Hz, allowing for the acquisition of a sufficient set of data for statistical analysis. Data similar to that presented in Fig. 134.27 are used: a set of 50 successive waveforms is measured, a temporal range where the pulse shape is not rapidly varying (i.e., avoiding the sharp leading and trailing edges) is isolated, the pulse shape over that range is normalized by a low-order fit, the rms and peak-to-valley variations of the normalized pulse are determined, and the global rms and peak-to-valley noise are obtained by averaging the values determined for each pulse. Using this procedure, the data of Fig. 134.27(a) for the main pulse lead to rms and peak-to-valley noise of 2.3% and 13.2%, respectively. Using the same procedure on a 1-ns pulse from the picket channel leads to similar values for the rms and peak-to-valley noise, 2.8% and 13.5%, respectively. The remaining noise can be attributed to measurement noise, imperfect amplitude and dispersion compensation, propagation effects in polarization-maintaining fibers, and etaloning in optical components. Amplitude noise caused by broadband analog-to-digital conversion by the oscilloscope is likely to be the largest contributor: direct measurement of a cw laser with the same photodetection led to rms and peak-to-valley amplitude noise of 1.6% and 9.6%, respectively, in a 3-ns time window. The measured noise is acceptable, considering the noise budget for the entire laser system, which requires less than a 20% peak-to-valley noise in the front end. Apart from the broadband noise from the photodetection system, the spectrum of the measured waveforms typically has low-density tones at the modulation frequencies. A parabolic spectral-amplitude modulation and high-order spectral phase modulations can lead to intermodulation components, i.e., sidebands of equal amplitude at the sum and difference of the modulation frequencies. The sum terms (e.g., $2f_3 \sim 63.8$ GHz and $f_1 + f_3 \sim 53.1$ GHz for the picket channel) are beyond the photodetection bandwidth, but the difference terms (e.g., $f_3 - f_1 \sim 10.7$ GHz) correspond to a high value of the detection frequency reponse. No significant spectral components at the difference frequencies have been observed when the amplitude compensator is adequately set, giving confidence in the spectral-amplitude compensation and showing that the impact of high-order terms in the spectral phase is negligible. These aspects will be studied in detail in the future. These experiments confirm that AM compensation to an acceptable noise level can be obtained simultaneously on the two channels.

A diffraction grating mounted inside the PAM is required for SSD: the angular dispersion (frequency versus wave vector

in the near field) of a phase-modulated pulse leads to a time-varying speckle distribution in the far field of the focusing lens after frequency conversion and random spatial-phase modulation from a phase plate.[6] The current system has a 1700-l/mm diffraction grating mounted in the Littrow configuration. The groove density is a trade-off between smoothing, pulse-shape, and laser requirements. A larger angular dispersion leads to more smoothing in the far field, but it temporally broadens the pulse shape. Angular dispersion widens the far field of the optical pulse, which can disrupt the propagation of the amplified pulse in vacuum spatial filters that re-image the beam throughout the laser system. Pinholes in vacuum spatial filters are designed to spatially filter the high spatial frequencies of the beam as it propagates in the laser system, but they can lead to spectral clipping of the spectrum of angularly dispersed phase-modulated pulses, which adds amplitude modulation in the time domain.

The tightest pinhole in the entire laser system is located in the PAM. The full optical spectrum was observed in the far field after that pinhole,[13] but amplitude noise was measured at an image plane of the diffraction grating after this pinhole to confirm that no amplitude noise is added to the front-end pulses. A PZ fiber was used to probe the laser beam, which has an ~2-cm size in that plane. Figure 134.34 displays the amplitude noise as a function of the longitudinal distance relative to a reference position. The noise is expected to be minimal at the image plane and to increase before and after the image plane.[20] The minimum noise should be equal to the noise before angular dispersion. The measured rms and peak-to-valley noise at the output of the regenerative amplifier (i.e., before the diffraction grating) were 2.8% and 14.2%, respectively, in good agreement with the minimum values observed at the image plane, 2.5% and 13.5%. The lower noise observed at the image plane is not fully understood, but it could be a result of a slight mismatch in the dispersion compensation: propagation away from the image plane is equivalent to second-order dispersion;[20] therefore a signal with a small amount of dispersion has lower amplitude noise when measured at a longitudinal distance slightly offset from the image plane.

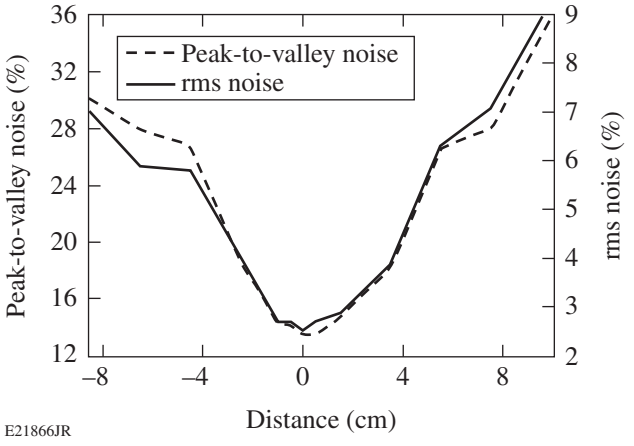

Figure 134.34
Amplitude noise (dashed line: peak-to-valley noise; solid line: rms noise) measured as a function of the longitudinal distance close to an image plane of the diffraction grating.

Conclusion

The front end demonstrates the use of high-bandwidth pulse shaping and phase modulation for high-energy laser systems. In particular, high-bandwidth, three-section phase modulators have been calibrated at microwave frequencies up to 40 GHz and routinely used at frequencies ranging from 3 to 32 GHz. The optical combination of optical pulses with different pulse shapes and phase modulations has made it possible to generate complex optical fields. Fail-safe systems have been used to detect the presence of adequate phase modulation and sufficient optical power at the output of the front end. A grating compressor and a Lyot filter have been used to decrease the FM-to-AM conversion caused by dispersive propagation and spectrally dependent amplifier gain. Pulse shape and noise measurements at frequencies up to 45 GHz have confirmed the accuracy of the compensation and adequacy of the system for seeding a high-energy laser system.

The front end has been used to generate seed pulses with a variety of shapes and phase modulations for the OMEGA EP Laser System to study the amplification, frequency-conversion, and beam-smoothing properties of these pulses.[13] The front end and associated technologies have made it possible to validate the multi-FM approach for beam smoothing and its application to a large-scale laser system. Implementation on a multibeam system will require significant multiplexing of the resources in the front end (particularly cw lasers, AWG's, and modulators) to minimize the associated space and cost. The 48 PAM's on the NIF might require seeding with optical pulses that have different shapes and central wavelength[1,11] requiring different front-end outputs, but building 48 front ends identical to the one described here would be prohibitive.

ACKNOWLEDGMENT

The authors thank M. W. Bowers, D. F. Browning, and G. V. Erbert (Lawrence Livermore National Laboratory) for fruitful discussions and assistance with NIF-related equipment, and T. J. B. Collins, J. H. Kelly, B. E. Kruschwitz, J. A. Marozas, and A. Shvydky (LLE) for fruitful discussions. This work was supported by the U.S. Department of Energy Office of Inertial Confinement Fusion under Cooperative Agreement No. DE-FC52-08NA28302, the Univer-

sity of Rochester, and the New York State Energy Research and Development Authority. The support of DOE does not constitute an endorsement by DOE of the views expressed in this article.

REFERENCES

1. C. A. Haynam *et al*., Appl. Opt. **46**, 3276 (2007).
2. N. Fleurot, C. Cavailler, and J. L. Bourgade, Fusion Eng. Des. **74**, 147 (2005).
3. J. D. Lindl, Phys. Plasmas **2**, 3933 (1995).
4. J. D. Kilkenny, S. G. Glendinning, S. W. Haan, B. A. Hammel, J. D. Lindl, D. Munro, B. A. Remington, S. V. Weber, J. P. Knauer, and C. P. Verdon, Phys. Plasmas **1**, 1379 (1994).
5. R. L. McCrory, D. D. Meyerhofer, R. Betti, R. S. Craxton, J. A. Delettrez, D. H. Edgell, V. Yu Glebov, V. N. Goncharov, D. R. Harding, D. W. Jacobs-Perkins, J. P. Knauer, F. J. Marshall, P. W. McKenty, P. B. Radha, S. P. Regan, T. C. Sangster, W. Seka, R. W. Short, S. Skupsky, V. A. Smalyuk, J. M. Soures, C. Stoeckl, B. Yaakobi, D. Shvarts, J. A. Frenje, C. K. Li, R. D. Petrasso, and F. H. Séguin, Phys. Plasmas **15**, 055503 (2008).
6. S. Skupsky, R. W. Short, T. Kessler, R. S. Craxton, S. Letzring, and J. M. Soures, J. Appl. Phys. **66**, 3456 (1989).
7. J. E. Rothenberg, J. Opt. Soc. Am. B **14**, 1664 (1997).
8. T. R. Boehly, D. L. Brown, R. S. Craxton, R. L. Keck, J. P. Knauer, J. H. Kelly, T. J. Kessler, S. A. Kumpan, S. J. Loucks, S. A. Letzring, F. J. Marshall, R. L. McCrory, S. F. B. Morse, W. Seka, J. M. Soures, and C. P. Verdon, Opt. Commun. **133**, 495 (1997).
9. S. Skupsky and R. S. Craxton, Phys. Plasmas **6**, 2157 (1999).
10. J. R. Murray *et al*., J. Opt. Soc. Am. B **6**, 2402 (1989).
11. T. J. B. Collins, J. A. Marozas, K. S. Anderson, R. Betti, R. S. Craxton, J. A. Delettrez, V. N. Goncharov, D. R. Harding, F. J. Marshall, R. L. McCrory, D. D. Meyerhofer, P. W. McKenty, P. B. Radha, A. Shvydky, S. Skupsky, and J. D. Zuegel, Phys. Plasmas **19**, 056308 (2012).
12. D. N. Maywar, J. H. Kelly, L. J. Waxer, S. F. B. Morse, I. A. Begishev, J. Bromage, C. Dorrer, J. L. Edwards, L. Folnsbee, M. J. Guardalben, S. D. Jacobs, R. Jungquist, T. J. Kessler, R. W. Kidder, B. E. Kruschwitz, S. J. Loucks, J. R. Marciante, R. L. McCrory, D. D. Meyerhofer, A. V. Okishev, J. B. Oliver, G. Pien, J. Qiao, J. Puth, A. L. Rigatti, A. W. Schmid, M. J. Shoup III, C. Stoeckl, K. A. Thorp, and J. D. Zuegel, J. Phys. Conf. Ser. **112**, 032007 (2008).
13. "Commissioning of a Multiple-Frequency–Modulation Smoothing by Spectral Dispersion Demonstration System on OMEGA EP," published in this volume.
14. V. N. Goncharov, T. C. Sangster, T. R. Boehly, S. X. Hu, I. V. Igumenshchev, F. J. Marshall, R. L. McCrory, D. D. Meyerhofer, P. B. Radha, W. Seka, S. Skupsky, C. Stoeckl, D. T. Casey, J. A. Frenje, and R. D. Petrasso, Phys. Rev. Lett. **104**, 165001 (2010).
15. P. J. Wisoff *et al*., in *Optical Engineering at the Lawrence Livermore National Laboratory II: The National Ignition Facility*, edited by M. A. Lane and C. R. Wuest (SPIE, Bellingham, WA, 2004), Vol. 5341, pp. 146–155.
16. M. Bowers *et al*., in *Solid State Lasers XVI: Technology and Devices*, edited by H. J. Hoffman, R. K. Shori, and N. Hodgson (SPIE, Bellingham, WA, 2007), Vol. 6451, p. 64511M.
17. J. K. Crane *et al*., in *Solid State Lasers for Application to Inertial Confinement Fusion: Second Annual International Conference*, edited by M. L. André (SPIE, Bellingham, WA, 1997), Vol. 3047, pp. 601–609.
18. D. Penninckx *et al*., J. Lightwave Technol. **24**, 4197 (2006).
19. J. E. Rothenberg, D. F. Browning, and R. B. Wilcox, in the *Third International Conference on Solid State Lasers for Application to Inertial Confinement Fusion*, edited by W. H. Lowdermilk (SPIE, Bellingham, WA, 1999), Vol. 3492, pp. 51–61.
20. S. Hocquet *et al*., Appl. Opt. **47**, 3338 (2008).
21. B. Lyot, C. R. Acad. Sci. (Paris) **197**, 1593 (1933).